machines

MDPI

Article

Active Disturbance Rejection Control of Engine Speed in Series Hydraulic Hybrid Power System

Zhiqiang Guo [1,*], Junlin Luo [2] and Yuwei Liu [1]

[1] School of Mechanical and Electrical Engineering, China University of Mining and Technology-Beijing, Beijing 100083, China
[2] China North Vehicle Research Institute, Beijing 100072, China
* Correspondence: gzqiang@cumtb.edu.cn

Abstract: In this paper, a novel series hydraulic hybrid powertrain is proposed for a three-axis all-terrain vehicle. The engine drives two variable displacement pumps responsible for driving and steering, respectively. A variable displacement motor is connected to the ring gear of the planetary coupling mechanism to drive the vehicle and a fixed-displacement motor is connected to the sun gear to steer the vehicle. The active disturbance rejection control with feedforward control is employed to control the engine speed. The engine speed is controlled in a close-looped manner by adjusting the engine throttle. The controller parameters are decided by analyzing the influence of each parameter on the controller performance by means of the control variable method. The simulation results indicate that the proposed control strategy enables the vehicle to obtain better engine speed following and anti-disturbance performance. An all-terrain prototype is established and field tests are carried out to verify the effectiveness of the design and control strategy of the series hydraulic hybrid powertrain for the all-terrain vehicle.

Keywords: hydraulic hybrid powertrain; active disturbance rejection control; all-terrain vehicles; engine speed control

check for updates

Citation: Guo, Z.; Luo, J.; Liu, Y. Active Disturbance Rejection Control of Engine Speed in Series Hydraulic Hybrid Power System. *Machines* **2024**, *12*, 733. https://doi.org/10.3390/machines12100733

Academic Editor: Zheng Chen

Received: 11 September 2024
Revised: 8 October 2024
Accepted: 14 October 2024
Published: 16 October 2024

Copyright: © 2024 by the authors. Licensee MDPI, Basel, Switzerland. This article is an open access article distributed under the terms and conditions of the Creative Commons Attribution (CC BY) license (https://creativecommons.org/licenses/by/4.0/).

1. Introduction

The hybrid hydraulic application is a promising solution to reduce the energy consumption and regenerate the braking energy of off-road vehicles [1–4], especially hydraulic excavators [5–7] and loaders [8]. Instead of a battery in the electric hybrid system, the hydraulic hybrid system employs a hydraulic accumulator to provide auxiliary power [9,10]. The accumulator has the advantage of a high power density and a low energy density.

As early as 1978, a hybrid hydrostatic drive system was developed in the Berlin Institute of Technology and it was tested on city buses; it was found that the fuel consumption was reduced by 20% to 29% [11,12]. After that, the regenerating potential of braking energy was validated by experimental tests based on a constant pressure system proposed by Mitsubishi. The results showed that the hybrid bus would recover 73% of kinetic energy at 20 km/h and reduce the exhaust emission and fuel consumption by more than 20% [13].

For hydraulic hybrid powertrains used in vehicles, there are three main configurations, the series hybrid system, the parallel hybrid system and the series–parallel hybrid system [14]. Justinus compared the power efficiency of hydrostatic transmission with a fixed-displacement or a variable-displacement motor in a series hybrid drive train with one pump or two pumps for a compact track loader. The results indicated that the one-pump series hybrid drive train saved the most fuel [15]. In most series hydraulic hybrid powertrains, two accumulators are applied. A high-pressure accumulator is adopted to store surplus engine energy and recover braking energy, as well as generate the torque for the system through a hydraulic pump/motor working in a specific mode, and a low-pressure accumulator is used to balance each cylinder flow [16,17]. A series hydraulic

hybrid powertrain is generally employed in wheel loaders. A series hybrid powertrain with one pump and two accumulators for a wheeled loader was investigated and an online optimization method was proposed and validated in reference [18]. An adaptive equivalent consumption minimization strategy for a compact series hydraulic hybrid wheel loader was presented to optimize the fuel economy in view of the repetitive work of the wheel loader [19]. Tri-Vien employed a model predictive controller to control a series hydraulic hybrid vehicle by regulating the vehicle velocity, the engine torque, the engine speed, as well as the accumulator pressure [20,21]. Wang placed emphasis on accumulator control by determining the working time of large and small accumulators to improve the vehicle fuel economy [22]. A simulation study proved that dynamic programming is helpful to obtain effective braking energy recovery and fuel economy [23]. A rule-based energy management strategy with control parameter selection based on dynamic programming was proposed to realize real-time control for a series hydraulic hybrid vehicle [24].

In previous studies, the series hybrid configuration was studied and used mostly on wheel loaders and trunks. The application of series hydraulic hybrid powertrains is also an effective approach for all-terrain vehicles. In addition, according to the construction of a series hydraulic hybrid powertrain, the engine and the hydraulic pump can be considered as a whole to provide the flow required by the hydraulic motor. The displacement of the hydraulic pump determines the engine load. Thus, an effective control strategy to control the engine speed is needed. In the present paper, the engine speed is controlled in a closed-loop manner with an ADRC by adjusting the engine throttle. Moreover, the proposed control strategy is verified in simulations and on an experimental vehicle.

The present paper is organized as follows. In Section 2, the series hydraulic hybrid powertrain for an all-terrain vehicle is introduced and presented. In Section 3, the active disturbance rejection control (ADRC) strategy to coordinate controlling the engine and hydraulic pump is proposed. In Section 4, the parameter choice method for the ADRC is conducted and the parameters adopted in this study are given. In Section 5.1, the simulation comparisons illustrate that the ADRC enables the vehicle engine speed to have better following and anti-disturbance performances. In Section 5.2, an all-terrain vehicle prototype is established and field tests verify the effectiveness of the design and the control of the series hydraulic hybrid powertrain in this paper. In the end, Section 5 draws conclusions on the present study and future work is envisaged.

2. System Configuration

A series hydraulic hybrid powertrain for a three-axis, all-wheel-drive, all-terrain vehicle is proposed in this paper. The configuration of the system is depicted in Figure 1. The vehicle power source is provided by a diesel engine. The system consists of two hydraulic circuits, called the driving hydraulic circuit and the steering hydraulic circuit, which are used for vehicle straight driving and vehicle steering, respectively. The driving hydraulic circuit is composed of an axial variable displacement pump (2), a high-pressure hydraulic accumulator (3), a low-pressure hydraulic accumulator (4) and an axial variable displacement motor (5). The steering hydraulic circuit is made up of an axial variable displacement pump (6) and a fixed-displacement motor (7). The output shafts of the driving hydraulic motor (5) and steering hydraulic motor (5) are connected to the ring gear and the sun gear of the planetary coupling mechanism, respectively. The left and right output shafts of the planetary coupling mechanism are connected to the left and right wheel sprockets, respectively, and then, all wheels are driven by a chain. There is no mechanical connection between the engine output shaft and the wheels, so the clutch was eliminated.

When the vehicle goes straight, the engine drives the hydraulic pump (2) through one slowdown gear and further drives the hydraulic motor (5). The output torque of the hydraulic motor is transmitted to the gear ring of the planetary gear mechanism through a two-stage gear. Finally, the wheels on two sides are driven by the planetary frames. A bidirectional variable pump is applied as the hydraulic pump (2). Thus, the vehicle can travel in advancing and reversing directions by changing the direction of the tilt angle

of the hydraulic pump. In addition, the engine also drives another hydraulic pump (6) to make the vehicle to steer. The steering hydraulic motor (7) relates to two sun gears of the planetary gear sets on two sides through a bevel gear and a spur gear. In this case, two sun gears will rotate in opposite directions, enabling the vehicle to carry out speed-difference-based steering.

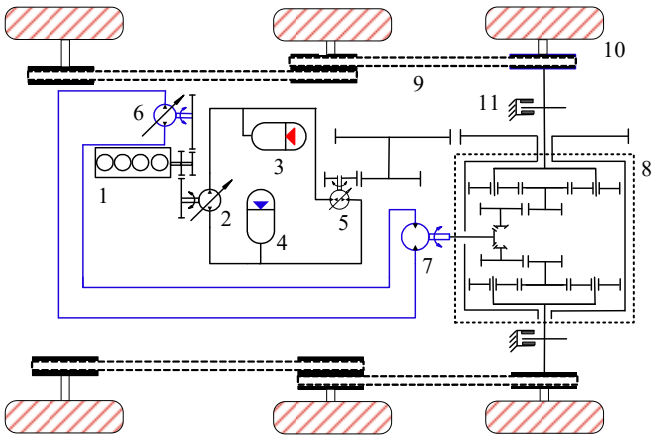

Figure 1. Configuration of hydraulic hybrid powertrain. 1—Engine. 2—Driving pump. 3—High-pressure hydraulic accumulator. 4—Low-pressure hydraulic accumulator. 5—Driving motor. 6—Steering pump. 7—Steering motor. 8—Planetary coupling mechanism. 9—Chain transmission. 10—Wheel. 11—Brake.

Under straight driving conditions, the working principle of the hydraulic drive system is depicted in Figure 2. Symbols P and M denote the two-way variable displacement pump and the variable displacement hydraulic motor, respectively. Two hydraulic accumulators are employed to regulate the engine load and recover the vehicle braking energy. A high-pressure accumulator and a low-pressure accumulator, respectively, denoted by HA and LA, are connected to the drive hydraulic circuit through two securing valves and a reversing valve. Symbol SV1 represents the four-way directional valve and it is initially set in the middle position, disconnecting the accumulators and the system hydraulic circuit. In this case, the vehicle works under hydrostatic continuously variable transmission. When the reversing valve is working on the right side, the high-pressure accumulator is connected to the A side of the system hydraulic circuit and the low-pressure accumulator is connected to the B side, enabling the vehicle to work under the hydraulic drive mode, the hybrid drive mode or the engine active charging mode. The vehicle will work under regenerating brake mode or reverse drive mode when the reversing valve works on the left side.

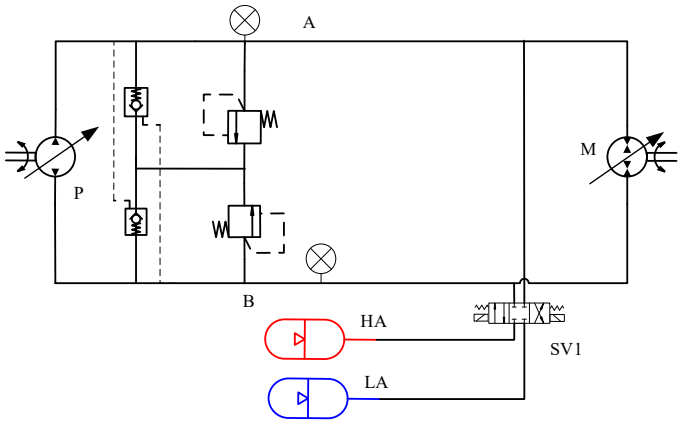

Figure 2. The straight driving hydraulic system.

A prototype using the proposed series hydraulic hybrid powertrain was established based on an all-terrain vehicle. The parameters of the tested vehicle are given in Table 1. The main components of the prototype are presented in Figure 3, namely the hydraulic motor, the hydraulic pump, the accumulator and powertrain assembly. The tested vehicle is shown in Figure 4.

Table 1. All-terrain vehicle prototype parameters.

Product Name	Specification	Parameter
Hydraulic pump	A10VG45EP4	Maximum displacement 45 mL/r
Hydraulic motor	A6VE80EP2	Maximum displacement 80 mL/r
Hydraulic accumulator	NXQ-A-10/31.5-L-Y	Nominal volume 10 L, initial pressure 10.5 MPa
Pressure transducer	MPM4842B-G-U4-401	Measuring range 0~40 MPa
Oil temperature sensor	MTMZ-PT1000	Measuring range −50~200 °C

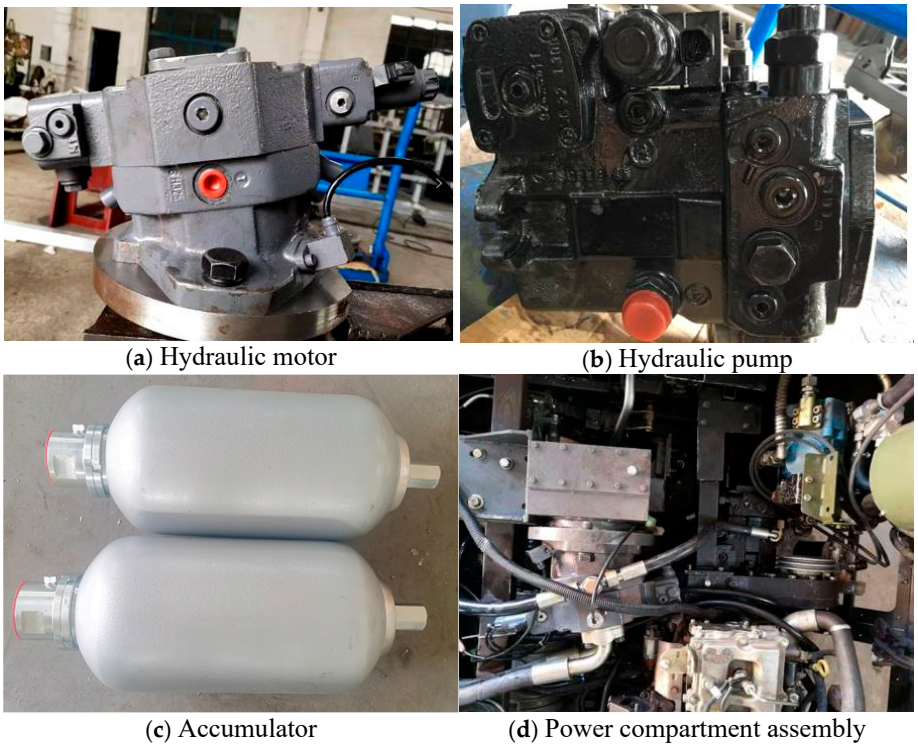

(**a**) Hydraulic motor (**b**) Hydraulic pump

(**c**) Accumulator (**d**) Power compartment assembly

Figure 3. Key components of the hydraulic hybrid power system.

Figure 4. Hydraulic hybrid test vehicle.

For the sake of clearer explanation, the control framework of the hydraulic vehicle is depicted in Figure 5, including the engine speed control, the hydraulic system pressure control and the hydraulic motor control. The displacement of the hydraulic pump is used to regulate the pressure of the hydraulic system. The displacement of the hydraulic motor is controlled based on the accelerator pedal and the feedback vehicle speed. The speed following the control performance of the engine is very important in a series hydraulic hybrid system because poor control could cause the engine to stall. This paper mainly studies the engine speed control strategy.

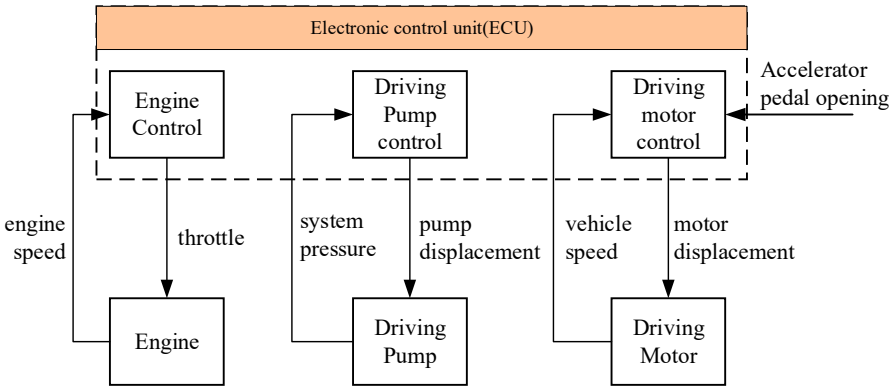

Figure 5. Hydraulic vehicle control framework.

3. Control Strategy

According to the system configuration, the engine speed affects the output flow of the hydraulic pump and the system pressure. In turn, the load torque of the engine is directly influenced by the hydraulic pump displacement and the system pressure. If the throttle control of the engine is inadequate, the engine would stall or suddenly increase, damaging ride comfort and fuel economy of the vehicle. Therefore, the control of the engine must have strong anti-interference and adaptive performance. In this paper, the active disturbance rejection control (ADRC) with the feedforward compensation is adopted to control the engine speed.

The engine speed control system is depicted in Figure 6. At first, the engine load can be estimated according to the drive system pressure, the steering system pressure, the steering angle and the displacement of the drive hydraulic pump. On account of engine torque characteristics, the feedforward control variable for engine throttle is computed. The ADRC system calculates the throttle correction based on the deviation between the target engine speed and the actual engine speed.

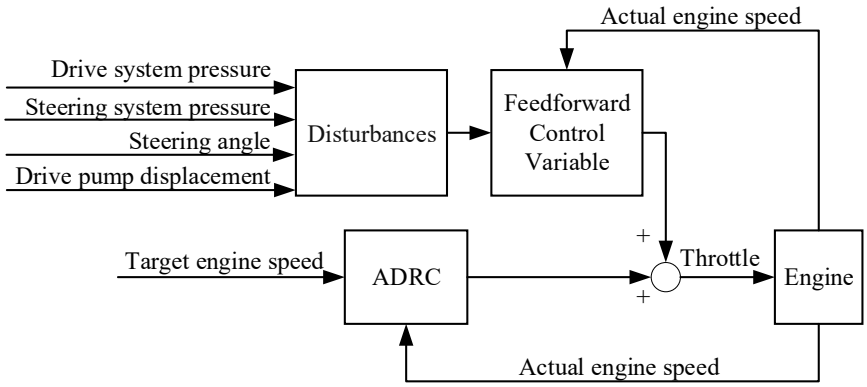

Figure 6. Engine speed control block diagram.

The feedforward part is employed to improve the accuracy and the anti-interference ability for the ADRC. In this system, the load torque of the engine is obtained by summing up the torques of the driving hydraulic pump and the steering hydraulic pump. The torque of the driving hydraulic pump and the torque of the steering hydraulic pump are calculated based on their displacements and pressures, respectively.

The engine load T_L can be estimated by the following equation:

$$T_L = \frac{\Delta P_s V_p}{2\pi i_e \eta_{pm} \eta_{ie}} + \frac{\Delta P_z V_{pz}}{2\pi i_{pz} \eta_{pzm} \eta_{ipz}} \quad (1)$$

where ΔP_s and ΔP_z are the pressure differences between the inlet and outlet for the driving hydraulic pump and steering hydraulic pump, respectively. Symbols V_p and V_{pz} are displacements of the driving and steering pumps, respectively. Symbols i_e and i_{pz} are transmission ratios between the engine output and the driving and steering pumps, respectively. Symbols η_{pm} and η_{pzm} are mechanical efficiencies of the driving and steering pumps, respectively. Symbols η_{ie} and η_{ipz} are transmission efficiencies of the driving and steering pumps, respectively.

Therefore, the feedforward control amount of the engine throttle can be obtained as:

$$\alpha_0 = \frac{T_L}{T_{e\max}(n_e)} \quad (2)$$

where α_0 denotes the feedforward adjustment for the engine throttle, $T_{e\max}(n_e)$ is the maximum engine torque at the current speed.

The ADRC was proposed by researcher Han Jingqing [25] on the basis of a PID controller. It has similar real-time performance and better anti-interference performance compared with the classical PID controller. The ADRC system is composed of a tracking differentiator (TD), an extended state observer (ESO), and Nonlinear State Error Feedback (NLSEF), as demonstrated in Figure 7. The tracking differentiator is designed to extract the target signal and its differential value, resulting in easier tuning and better robustness than the traditional PID controller. The extended state observer is in charge of estimating and compensating the disturbance in real time. The NLSFF is adopted to combine the error signal, the differential and the integral of error, which is easy to implement and has good robustness and adaptability. In Figure 7, symbols v_1 and v_2 are the follow signals of the target and the differential of target signal v, respectively. Symbols z_1 and z_2 are the follow signals of the feedback signal y of the controlled object and its differential signal, respectively. Symbol z_3 denotes the estimate of the system disturbance. Symbols e_1 and e_2 represent errors. Symbols u_0 and u are the control variable of the NLSFF and the control variable with compensation, respectively. The research object is controlled by the control variable u.

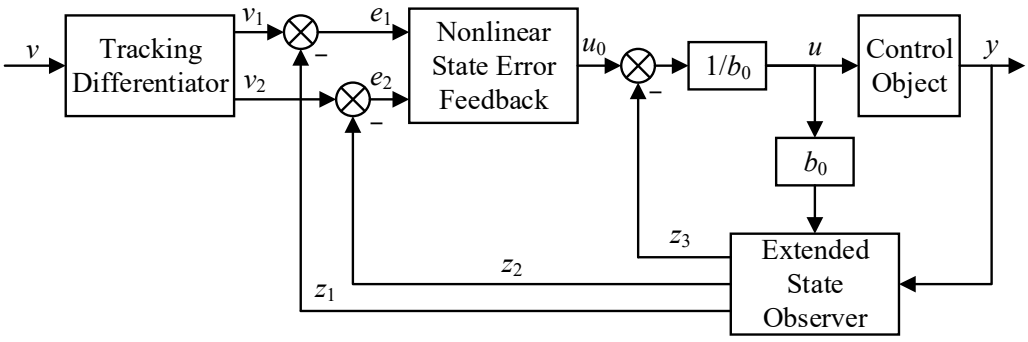

Figure 7. ADRC structure.

In this paper, the ADRC system is employed to control the engine speed, where the requirement speed of the engine is the target signal, the actual speed of the engine is the feedback signal and the engine throttle is the control object. Since that the ADRC is insensible of system model order, a low-order controller is usually adopted to control a high-order system [26]. Thus, the engine is considered as a second-order system and the second-order ADRC is designed as follows.

The second-order system is described as:

$$\ddot{y} = f(y, \dot{y}, \omega(t), t) + b_0 u \tag{3}$$

where y is the system output, $\dot{y}$ and $\ddot{y}$ are the derivative and second derivative of the system output, $\omega(t)$ is system disturbance, u is a control variable and b is control gain.

The state variables are defined as $x_1 = y$, $x_2 = \dot{y}$, and the second-order system can be expressed in a state equation as:

$$\begin{cases} \dot{x}_1 &= x_2 \\ \dot{x}_2 &= f(x_1, x_2, \omega(t), t) + b_0 u \\ y &= x_1 \end{cases} \tag{4}$$

where $f(x_1, x_2, \omega(t), t)$ is the total disturbance function of external and internal disturbance. The core of the ADRC design is to estimate the total disturbance and eliminate its influence.

Change Equation (4) into integral series standard form as:

$$\ddot{y} = u \tag{5}$$

To observe the system disturbance, the total disturbance is designed as a new state variable in the ESO module and presented as:

$$x_3(t) = f(x_1, x_2, \omega(t), t) \tag{6}$$

Thus, the second-order system is expressed as:

$$\begin{cases} \dot{x}_1 = x_2 \\ \dot{x}_2 = x_3 + b_0 u \\ \dot{x}_3 = \omega_0(t) \\ y = x_1 \end{cases} \tag{7}$$

Since a second-order ADRC consists of three parts [25], the disturbance estimation obtained by the ESO can be calculated by:

$$\begin{cases} e(k) = z_1(k) - y(k) \\ f_e = fal(e(k), 0.5, \delta) \\ f_{e1} = fal(e(k), 0.25, \delta) \\ z_1(k+1) = z_1(k) + h(z_2(k) - \beta_{01} e(k)) \\ z_2(k+1) = z_2(k) + h(z_3(k) - \beta_{02} f_e + bu(k)) \\ z_3(k+1) = z_3(k) + h(-\beta_{03} f_{e1}) \end{cases} \tag{8}$$

where $fal(x, a, \delta)$ is a nonlinear function and can be described as:

$$fal(x, a, \delta) = \begin{cases} \frac{x}{\delta^{(1-a)}}, & |x| \le \delta \\ sign(x)|x|^a, & |x| > \delta \end{cases} \tag{9}$$

Thus, the disturbance state variable x_3 is estimated by the observed z_3.

In this paper, the target engine speed is adopted as the input of the tracking differentiator. The calculation formulas of the tracking differentiator are presented as:

$$\begin{cases} fh = fhan(v_1(k) - v(k), v_2(k), r_0, h_0) \\ v_1(k+1) = v_1(k) + h \cdot v_2(k) \\ v_2(k+1) = v_2(k) + h \cdot fh \end{cases} \tag{10}$$

where h is sample time, h_0 is the filter factor of the tracking differentiator, r_0 is the speed factor to adjust the speed of the transition process, $v(k)$ is the reference signal at the moment of k. The function *fh* is the fast optimal control synthesis function and is expressed as:

$$\begin{aligned} &fh = fhan(x_1, x_2, r, h): \\ &\begin{cases} d = rh \\ d_0 = hd \\ y = x_1 + hx_2 \\ a_0 = \sqrt{d^2 + 8r|y|} \\ a = \begin{cases} x_2 + \frac{(a_0 - d)}{2} sign(y), |y| > d_0 \\ x_2 + \frac{y}{h}, |y| \le d_0 \end{cases} \\ fhan = -\begin{cases} rsign(a), |a| > d \\ r\frac{a}{d}, |a| \le d \end{cases} \end{cases} \end{aligned} \tag{11}$$

The NLSEF is designed based on the *fhan* function and presented as:

$$u_0 = fhan(e_1, c_1 e_2, r_1, h_1) \tag{12}$$

where c_1 is the damping factor and h_1 is the precision factor.

The control variable can be compensated by the disturbance estimation from the extended state observer as:

$$u(k) = u_0 - \frac{z_3(k)}{b_0} \tag{13}$$

According to the reference [26], the parameters β_{01}, β_{02} and β_{03} of the extended state observer can be preliminarily set by the sample step time as:

$$\beta_{01} = \frac{1}{h}, \beta_{02} = \frac{1}{1.6h^{1.5}}, \beta_{03} = \frac{1}{8.6h^{2.2}} \tag{14}$$

An electro-hydraulic servo actuator is employed to control the displacement of the hydraulic pump by changing the inclination angle of the pump swash plate. The target current is calculated by the pump displacement and a PI control strategy is adopted to follow the target current. The relationship between the desired current and the desired pump displacement can be expressed by:

$$I_{pr} = \frac{V_{pr}}{V_{p\max}} \left(I_{p\max} - I_{p\min} \right) + I_{p\min} \tag{15}$$

where V_{pr} is the desired displacement of the hydraulic pump, $I_{p\max}$ and $I_{p\min}$ are the maximum value and the minimum value of the control current, respectively. In this paper, the maximum current is 600 mA at maximum displacement and the minimum current is 200 mA at zero displacement.

4. Parameter Design

All parameters of the ADRC together determine the control results. In this paper, the control variable method is adopted to analyze the influence of each parameter on the controller performance and the controller parameters are decided. The simulation model of the hydraulic hybrid vehicle is established in AMESim Rev 13 software, as shown in Figure 8. Key parameters of the simulation model are presented in Table 2.

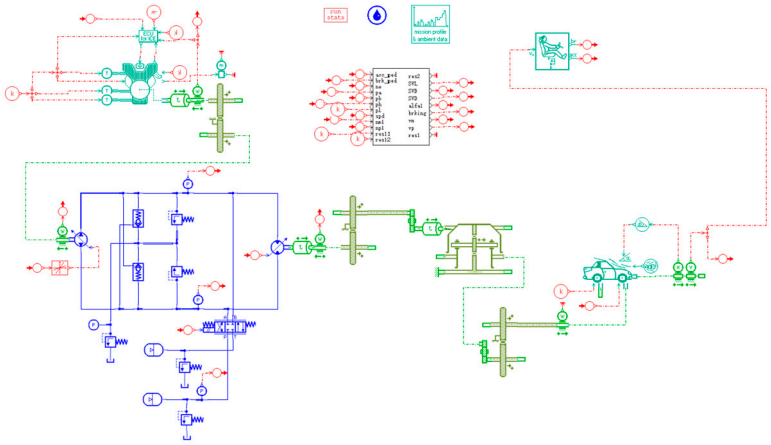

Figure 8. The hydraulic hybrid powertrain simulation model.

Table 2. Simulation model parameters.

Parameter	Value
Engine type	Compressed ignition
Maximum engine speed	4200 rpm
Maximum engine speed	192 Nm
i_e	1.27
i_{pz}	2000
Pump maximum displacement	45 cc/rev
Motor maximum displacement	80 cc/rev
Relief valve cracking pressure	300 bar

A step signal which jumps to 2400 r/min from 1000 r/min at the moment of 5 s is adopted as the target engine speed and the sample step time is set as 0.01 s. The hydraulic pump displacement is zero and the engine works without load. Figure 9 illustrates the results of the step responses when parameter h takes different values.

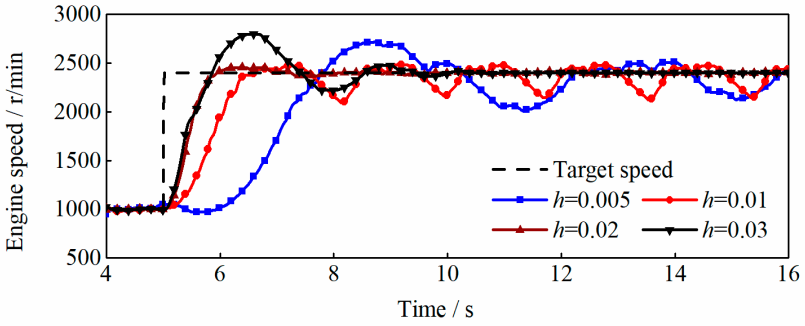

Figure 9. Effect of parameter h on engine speed following performance.

It can be found that parameter h affects the engine speed rise time, overshoot and steady-state error. When the value of parameter h increases from 0.005 to 0.03, the engine speed rise time first becomes shorter and then remains unchanged after h exceeds 0.02. In the meantime, the overshoot decreases first and then increases, the controller stability becomes better first and then becomes worse. When parameter h is set as 0.02, the rise time, overshoot and convergence rate are all satisfactory. Therefore, the value of parameter h should not be smaller than the sample step time of the controller. Besides, a larger h is needed when the actual engine speed fluctuates strongly near the target value.

Figure 10 shows the engine speed variations when the value of parameter r_1 is set different. The value of parameter r_1 has significate influence on the controller performance

because r_1 is one of the parameters in the NLSFF to determine the control variable. When r_1 is set as a small value, the engine speed overshoot and the settling time are both relatively large. The engine speed overshoot and settling time will become smaller when r_1 becomes bigger; however, their change is not obvious any more when r_1 exceeds 2000. Therefore, the value of parameter r_1 should not be very small.

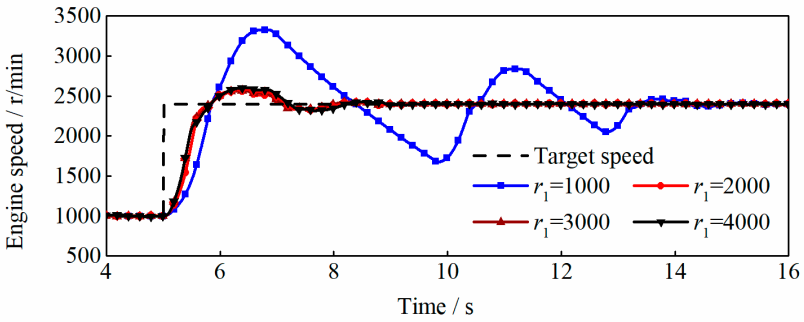

Figure 10. Effect of parameter r1 on engine speed following performance.

Figure 11 demonstrates the engine speed responses when parameter b_0 takes different values, and Figure 12 demonstrates the engine speed responses when parameter c_1 takes different values. When the value of parameter b_0 increases from 500 to 3000, the settling time of the engine speed becomes larger to a small extent and other indicators remain unchanged. When the value of parameter c_1 increases from 0.001 to 0.02, the engine speed variations basically coincide and the controller performance is not influenced.

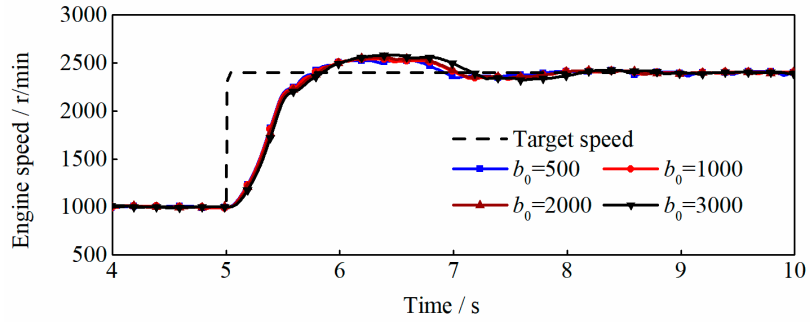

Figure 11. Effect of parameter b_0 on engine speed following performance.

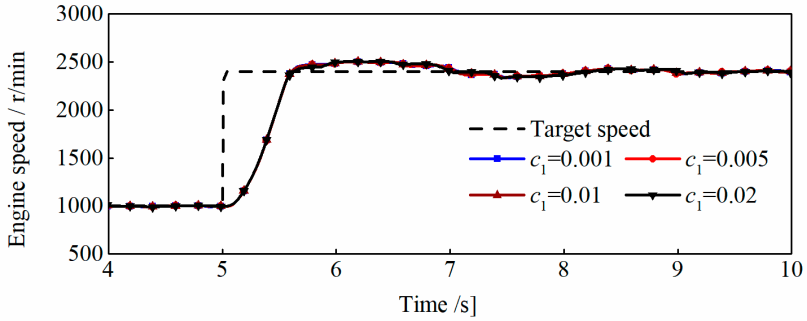

Figure 12. Effect of parameter c1 on engine speed following performance.

All parameters of ADRC are analyzed and the controller parameters are decided as shown in Table 3.

Table 3. ADRC parameters.

Parameter	Value
h	0.02
δ	$5 \times h$
r_1	3500
r_0	1000
b	2000
b_0	2000
h_0	$5 \times h$
h_1	$5 \times h$
c_1	0.01

5. Results and Discussion

5.1. Comparison with Traditional Control Strategy

The proposed ADRC is compared with a traditional PID controller to control the engine speed. Under the same conditions, the parameters of the PID controller are analyzed and decided. Figures 13 and 14 show the engine speed variations with different values for proportion factor k_p and different values for integration factor k_i, respectively. Thus, the proportion factor k_p is set as 0.008 and the integration factor k_i is set as 0.0001.

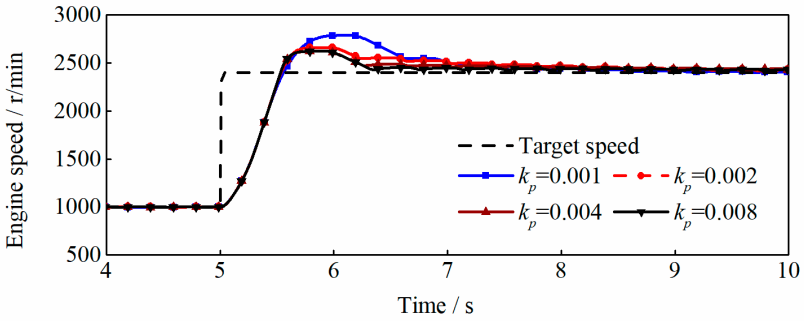

Figure 13. Choice of parameter kp for PID controller.

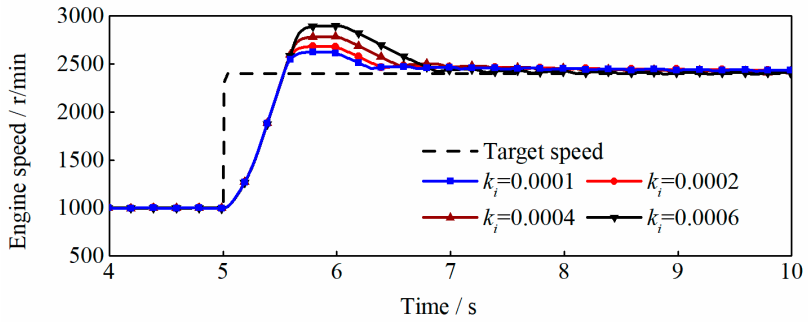

Figure 14. Choice of parameter ki for PID controller.

Figure 15 illustrates the engine speed variations with the proposed ADRC and the traditional PID controller when the target speed steps down to 1500 r/min from 3500 r/min at the moment of 5 s. The speed rise time for the ADRC is 0.98 s and that for the PID controller is 0.66 s. The PID controller has a more rapid response than the ADRC. This is because there is a transition process for the target signal, which restricts the controlled signal rise rate. Though the ADRC takes more time to respond, the overshoot and the settling time are reduced by 49.92% and 50.59%, respectively. The maximum engine speed is 3730 r/min with the PID controller and 3615 r/min with ADRC, respectively. The engine takes 8.5 s and 4.2 s to reach a steady state under the control of the PID controller and the ADRC, respectively. Therefore, the ADRC performance is better than the traditional PID controller under the step condition for the target engine speed.

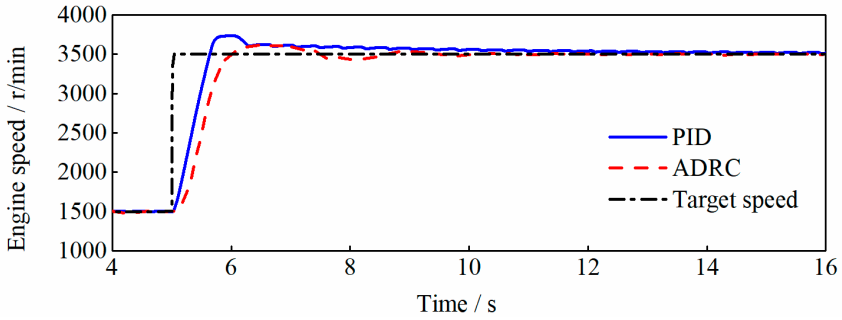

Figure 15. Engine speed step responses by means of ADRC and PID controllers.

When the displacement of the steering pump or driving pump suddenly increases, the engine speed will decrease. Figure 16 presents the control results when the target engine speed is set as 1500 r/min and the displacement of the hydraulic pump steps up to 0.6 from 0 at the time of 30 s. The engine speed decreases and then increases to the target speed under the control of two controllers. With the ADRC, the engine takes 2.7 s to rise back to the target speed and the minimum speed is 1380 r/min, while the engine takes 15.5 s and the minimum speed is 1296 r/min with the traditional PID controller. The comparisons prove that the engine speed control has better anti-disturbance performance through the ADRC system than the PID control. This is because the ADRC can estimate and compensate the system disturbance in real time.

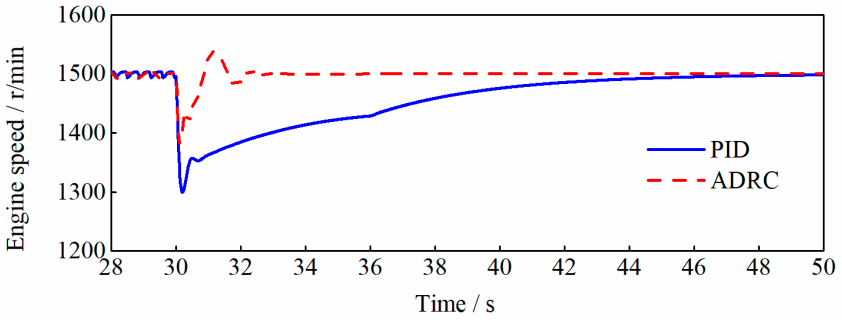

Figure 16. Engine speed responses under step load conditions.

A sinusoidal target engine speed is employed to verify the dynamic following ability of the engine speed under the load. Figure 17a,b show the engine speed results and the speed difference results with two controllers when the target engine speed is set as a sine function with the frequency of 2 rad/s, the amplitude of 200 r/min and the offset of 1500 r/min. It can be found that two controllers both enable the engine to follow the sinusoidal target speed. The maximum engine speed differences under the control of the PID controller and the ADRC are, respectively, 76 r/min and 40 r/min. The engine deviation under ADRC is 47.27% smaller than that under PID control.

In conclusion, the proposed ADRC has better control performance than the PID controller for the engine to follow the target speed under the step speed condition, the step load condition and the sinusoidal speed condition.

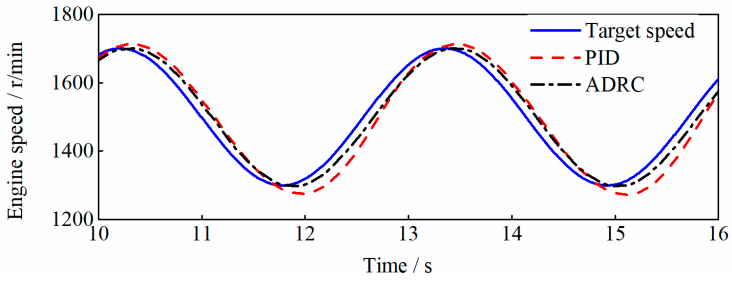

(a) Engine following speeds

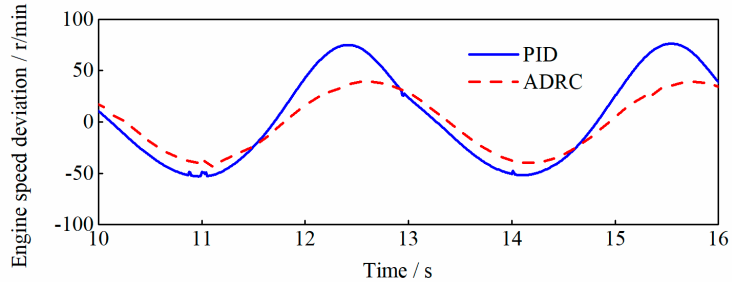

(b) Engine speed following deviations

Figure 17. Control for sinusoidal target engine speed.

5.2. Prototype-Tested Results

Simulink and Stateflow of Matlab R2014a are used to develop an algorithm model of the vehicle integrated control system. As depicted in Figure 18, the green part on the left is the signal input module to acquire and process the signals including the acceleration pedal opening, the brake pedal opening, the engine speed, the system pressure and the gear status. The middle orange module is the core control algorithm module of the vehicle, which is composed of the driver intention analysis, the mode switching logic, the hydraulic pump, the hydraulic motor, the engine and the reversing valve control. The blue module on the right is the signal output module, from where the proportional solenoid valve current drive of the hydraulic pump, hydraulic motor and the reversing valve drive can be obtained.

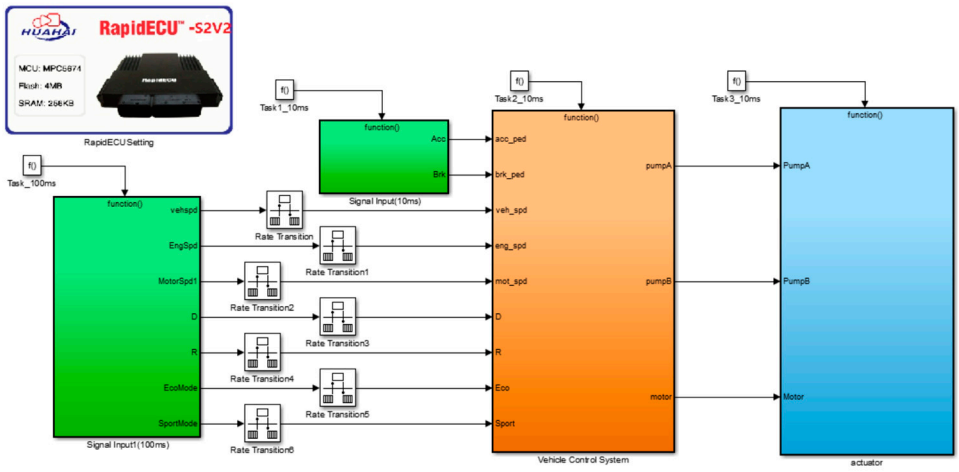

Figure 18. Simulink model of rapid prototype of controller.

A prototype vehicle using the proposed series hydraulic hybrid powertrain is used to validate the effectiveness of the proposed ADRC.

The tested vehicle accelerates from 0 to 40 km/h and then maintains the vehicle speed within the regular speed range of 30–40 km/h. Figure 19 illustrates the tested vehicle velocity variations. It shows that the tested vehicle could drive steadily at a normal speed

and that the velocity could be maintained at 30–40 km/h. Figure 20 shows the tested pressures of the inlet and outlet of the hydraulic motor. The target pressure of the system is 20 MPa and it can be seen that the p_A could be maintained near the target pressure with a small fluctuation. This is because the driving resistance, the vehicle speed and the throttle signal provided by the driver acceleration pedal are time-varying when the vehicle is travelling in reality, resulting in changing the required flow for the hydraulic motor. In addition, there is a delay before the outlet displacement of the hydraulic pump. Thus, the system pressure showed a fluctuation to a certain extent. The p_B stayed at around 2 MPa, indicating that the oil replenishment system worked properly.

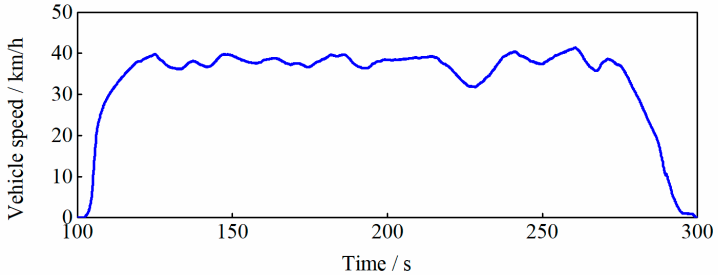

Figure 19. Experimental vehicle speed.

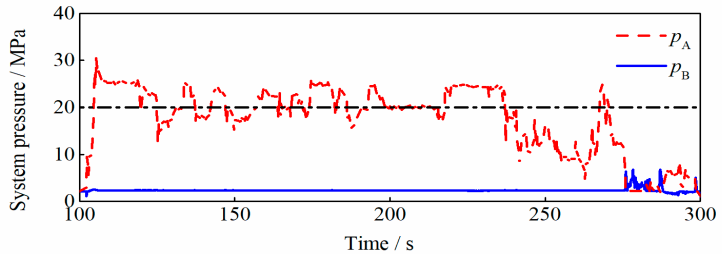

Figure 20. Highway driving test pressure curve.

The engine speed variations of the tested vehicle are drawn in Figure 21. It can be found that the engine worked at nearly 2200 r/min, verifying the effectiveness of the proposed engine follow control strategy. There is a significant overshoot in the control of engine speed on the step transient from 1000 to 2000 r/min. This is because the proposed coordinated control strategy preferentially adjusts the engine speed to the target speed to avoid engine stalling. When the vehicle begins to accelerate rapidly, the hydraulic pump needs to rise quickly to meet the motor flow demand. However, the rapid rise of the hydraulic pump can easily cause the engine to stall, especially at a low speed. Therefore, the rapid increase of the engine speed is meant to provide the hydraulic pump with a faster speed, thereby increasing the pump's output flow. During the process of starting the vehicle, it takes some time for the hydraulic system to establish pressure, resulting in a relatively small load on the engine and causing an overshoot.

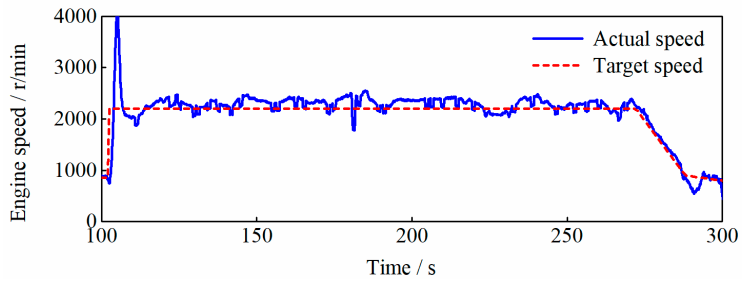

Figure 21. Experimental engine speed.

According to the system pressure and the engine speed, the calculation indicated that the engine operated in the high-efficiency zone. Thus, the proposed controller enables the vehicle to have good economy performance.

Figure 22 displays the engine throttle variations. Comparing Figure 22 with Figure 20, it can be seen that the throttle was changing with the system pressure. The system pressure increased when the engine throttle increased and the system pressure became smaller when the throttle was reduced. This means that the system pressure could be maintained by means of adjusting the engine throttle. Therefore, the proposed control strategy is validated by the uniform speed driving experiment.

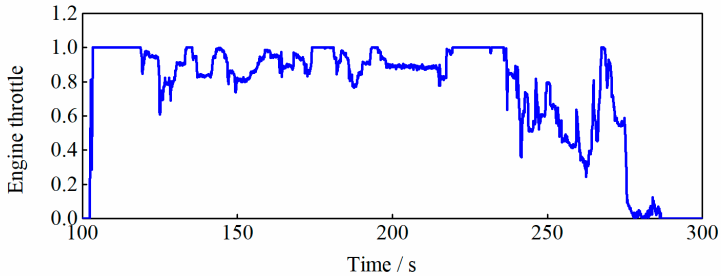

Figure 22. Experimental engine throttle.

6. Conclusions

In this study, a novel series hydraulic hybrid powertrain is employed in an all-terrain vehicle and the active disturbance rejection control strategy is proposed to control the engine. The ADRC is verified by a field test through a prototype. The results suggest the following:

(1) This paper proposes an ADRC system with feedforward for the engine speed control in a series hydraulic hybrid power system and introduces the influence laws of its controller parameters.
(2) Compared with the traditional PID controller, the ADRC enables the engine to follow the target speed better under the step speed conditions, the step load conditions and the sinusoidal speed conditions.
(3) The tested all-terrain vehicle could drive at a uniform velocity under the control of the proposed ADRC strategy. The engine speed could follow the target speed satisfactorily.

In future studies, the regenerating potential and effective control method of braking energy for the all-terrain vehicle could be taken into account on the basis of the proposed series hydraulic hybrid powertrain.

Author Contributions: Data curation, J.L.; funding acquisition, Z.G.; investigation, Z.G.; methodology, J.L.; software, Y.L.; validation, J.L.; writing—original draft, Z.G.; writing—review and editing, Y.L. All authors have read and agreed to the published version of the manuscript.

Funding: This work was supported by the National Natural Science Foundation of China [grant number 52302484] and the National Key Laboratory Fund Project [grant number NKL20811202301017230207].

Data Availability Statement: Data are unavailable due to privacy.

Conflicts of Interest: The authors declare no conflicts of interest.

References

1. Midgley, W.J.; Abrahams, D.; Garner, C.P.; Caldwell, N. Modelling and experimental validation of the performance of a digital displacement® hydraulic hybrid truck. *Proc. Inst. Mech. Eng. Part D J. Automob. Eng.* **2022**, *236*, 594–605. [CrossRef]
2. Zhou, S.; Walker, P.; Zhang, N. Parametric design and regenerative braking control of a parallel hydraulic hybrid vehicle. *Mech. Mach. Theory* **2020**, *146*, 103714. [CrossRef]
3. Zhou, S.; Walker, P.; Wu, J.; Zhang, N. Power on gear shift control strategy design for a parallel hydraulic hybrid vehicle. *Mech. Syst. Signal Pr.* **2021**, *159*, 107798. [CrossRef]

4. Li, H.; Zhu, D.; Shang, L.; Fan, P. Research on an energy management strategy and energy optimisation of hydraulic hybrid power mining trucks. *Int. J. Veh. Des.* **2022**, *85*, 246–273. [CrossRef]
5. Xiao, Y.; Guan, C.; Lai, X. Research on the design and control strategy for a flow-coupling-based hydraulic hybrid excavator. *Proc. Inst. Mech. Eng. Part D J. Automob. Eng.* **2014**, *228*, 1675–1687. [CrossRef]
6. Yu, Y.; Do, T.C.; Yin, B.; Ahn, K.K. Improvement of Energy Saving for Hybrid Hydraulic Excavator with Novel Powertrain. *Int. J. Precis. Eng. Manuf. Technol.* **2023**, *10*, 521–534. [CrossRef]
7. Ge, L.; Dong, Z.; Quan, L.; Li, Y. Potential energy regeneration method and its engineering applications in large-scale excavators. *Energy Convers. Manag.* **2019**, *195*, 1309–1318. [CrossRef]
8. Mu, H.; Luo, Y.; Luo, Y.; Chen, L. Numerical Analysis of Energy Recovery of Hybrid Loader Actuators Based on Parameters Optimization. *Actuators* **2022**, *11*, 260. [CrossRef]
9. Zhang, W.; Wang, J.; Du, S.; Ma, H.; Zhao, W.; Li, H. Energy Management Strategies for Hybrid Construction Machinery: Evolution, Classification, Comparison and Future Trends. *Energies* **2019**, *12*, 2024. [CrossRef]
10. Prado Barbosa, T.; de Faria Lemos, A.; Ferreira Gonçalves, L.O.; Martins Ferreira, R.P.; Rodrigues da Silva, L.A.; Horta Gutiérrez, J.C. Optimization Tools Applied in the Design of a Hydraulic Hybrid Powertrain for Minimal Fuel Consumption. In *International Symposium on Multibody Systems and Mechatronics*; Springer: Cham, Switzerland, 2022.
11. Thier, T.; Benneter, B. Hydro-Bus—A City Bus with Hydrostatic Regenerative Braking. *Automobiltech Z* **1978**, *80*, 597–600.
12. Willumeit, H.P.; Benneter, B. Hydro-Bus—A City Bus with Braking-Recovery System. In *Publication of Society of Automotive Engineers*; Society of Automotive Engineers: Warrendale, PA, USA, 1982.
13. Hiroki, S.; Shigeru, I.; Eitaro, K. Study on Hybrid Vehicle Using Constant Pressure Hydraulic System with Flywheel for Energy Storage. In *Powertrain and Fluid Systems Conference and Exhibition*; SAE Technical Paper 2004-01-3064; SAE International: Warrendale, PA, USA, 2004.
14. Hubertus, M.; Edgar, W. Recent Developments for the Control of Variable Displacement Motors with Impressed Pressure. In Proceedings of the 3th JHPS International Symposium on Fluid Power, Yokohama, Japan, 4–6 November 1996; pp. 79–84.
15. Hartoyo, J.K.; Li, P.Y. Optimal Control and Architecture Design Optimization for Hydraulic Drive Train of a Compact Track Loader. In Proceedings of the Annual American Control Conference, Virtual, 25–28 May 2021.
16. Hippalgaonkar, R.; Ivantysynova, M. A Series-Parallel Hydraulic Hybrid Mini-Excavator with Displacement Controlled Actuators. In Proceedings of the 13th Scandinavian International Conference on Fluid Power, Linköping, Sweden, 3–5 June 2013.
17. Zimmerman, J.; Hippalgaonkar, R.; Ivantysynova, M. Optimal control for the series-parallel deplacemant controlled hydraulic hybrid excavator. In Proceedings of the ASME Dynamic Systems and Control Conference and Bath/Asme Symposium on Fluid Power and Motion Control, Arlington, VA, USA, 31 October–2 November 2012.
18. Zhang, Q.; Wang, F.; Xu, B.; Sun, Z. Online optimization of Pontryagin's minimum principle for a series hydraulic hybrid wheel loader. *Proc. Inst. Mech. Eng. Part D J. Automob. Eng.* **2022**, *236*, 1487–1499. [CrossRef]
19. Wen, Q.; Wang, F.; Cheng, M.; Xu, B.; Sun, Z. Adaptive Equivalent Consumption Minimization Strategy for Off-Road Hydraulic Hybrid Vehicles: A Cycle-to-Cycle Optimization Approach. *IEEE Trans. Veh. Technol.* **2022**, *71*, 2346–2357. [CrossRef]
20. Vu, T.V.; Chen, C.K. A Model-Based Controller Development for a Series Hydraulic Hybrid Vehicle. In Proceedings of the International Conference on Advanced Engineering Theory and Applications, Busan, Republic of Korea, 8–10 December 2016; Springer: Cham, Switzerland, 2016.
21. Vu, T.V.; Chen, C.K.; Hung, C.W. A Model Predictive Control Approach for Fuel Economy Improvement of a Series Hydraulic Hybrid Vehicle. *Energies* **2014**, *7*, 7017–7040. [CrossRef]
22. Wang, B.; Cheng, F.R.; Tang, X.Z. Research on the complete vehicle control strategy of the composite accumulator hydraulic hybrid power system. *J. Energy Storage* **2023**, *74*, 109384. [CrossRef]
23. Hung, C.W.; Vu, T.V.; Chen, C. The Development of an Optimal Control Strategy for a Series Hydraulic Hybrid Vehicle. *Appl. Sci.* **2016**, *6*, 93. [CrossRef]
24. Zhou, H.; Xu, Z.; Liu, L.; Liu, D.; Zhang, L. A Rule-Based Energy Management Strategy Based on Dynamic Programming for Hydraulic Hybrid Vehicles. *Math. Probl. Eng.* **2018**, *7*, 9492026. [CrossRef]
25. Han, Z.Q. *The Technique for Estimating and Compensating the Uncertainties*; National Defence Industry Press: Arlington, VA, USA, 2008.
26. Zhu, B. *Introduction to Active Disturbance Rejection Control*; Beijing University of Aeronautics and Astronautics Press: Beijing, China, 2017.

Disclaimer/Publisher's Note: The statements, opinions and data contained in all publications are solely those of the individual author(s) and contributor(s) and not of MDPI and/or the editor(s). MDPI and/or the editor(s) disclaim responsibility for any injury to people or property resulting from any ideas, methods, instructions or products referred to in the content.